Spatiotemporal effects on squeezing measurements

Filippus S. Roux *

National Metrology Institute of South Africa, Meiring Naudé Road, Brummeria 0040, Pretoria, South Africa

(Received 21 September 2020; accepted 14 December 2020; published 5 January 2021)

The role of the spatiotemporal degrees of freedom in the preparation and observation of squeezed photonic states, produced by parametric down-conversion, is investigated. The analysis is done with the aid of a functional approach under the semiclassical approximation and the thin-crystal approximation. It is found that the squeezed state loses its minimum uncertainty property as the efficiency of down-conversion is increased, depending on the conditions of the homodyne measurements with which the amount of squeezing is determined.

DOI: 10.1103/PhysRevA.103.013701

I. INTRODUCTION

Squeezed vacuum states [1,2] are among the most useful quantum states. They are used to make measurements that are more precise than the standard quantum limit (the shot-noise limit) would allow. For this reason, they are used in various applications, ranging from quantum computing to gravitational wave detection [3–9].

In quantum optics, squeezed vacuum states can be produced with the aid of nonlinear optical processes, such as parametric down-conversion [10]. Although challenging to analyze, parametric down-conversion has been studied for decades and much progress has been made in its analytical representation [11–18].

A squeezed vacuum state can be represented by a squeezing operator applied to the vacuum. Without the spatiotemporal degrees of freedom, the squeezing operator is parameterized by a single parameter, called the *squeezing parameter*. The inclusion of the spatiotemporal degrees of freedom causes the squeezed vacuum states to become a complex combination of *squeezing eigenmodes*, each with its own squeezing parameter [12].

To incorporate the spatiotemporal degrees of freedom in down-converted squeezed vacuum states, the squeezing operator is often expressed in terms of a set of ladder operators (or quadrature operators) in which each operator pair is associated with one of the eigenmodes [12,17,18]. It leads to a symplectic formalism where the squeezing operator is represented as a Gaussian operator—an exponential with an argument that is second order in ladder (or quadrature) operators [4–7].

The versatility of the symplectic formalism is demonstrated by its use in numerous analyses of the parametric down-conversion process and its applications. It represents the kernels of the down-conversion process as matrices that can be diagonalized with a Bloch-Messiah reduction [19]. Such a representation assumes a discrete finite-dimensional system. The down-conversion process can also be represented in terms of a Magnus expansion [20,21]. The symplectic matrix representation usually involves only the first order in the Magnus expansion [18].

Moreover, the matrix representation associated with the Bloch-Messiah reduction assumes knowledge of the eigenmodes (or Schmidt basis) of the kernels. However, the exact nature of these eigenmodes are not known and has so far only been obtained approximately by employing simplifying assumptions [13,14].

The applicability of the symplectic formalism and the Bloch-Messiah reduction in the analysis of the parametric down-conversion process is largely limited to those cases where the pump can be represented as a classical field, variously called the *semiclassical approximation*, the *parametric approximation*, the *undepleted pump approximation*, among others. (An exception is where it is used for a depleted pump scenario in a waveguide coupler [22].) The justification for this approximation is that the efficiency of the process is low enough that the pump remains unaffected (undepleted).

Recently, a functional formalism was used to analyze the down-conversion process, incorporating all spatiotemporal degrees of freedom [23]. The functional formalism operates directly with the kernels of the down-conversion process and does not need to represent them as finite-dimensional matrices. It avoids the need for knowledge of the eigenmodes by expressing any final result (such as what would be obtained in a measurement) directly in terms of the kernels. The functional formalism also allows calculations beyond the semiclassical approximation, using a perturbative process. It reproduces the expressions of the semiclassical part of the solution (zeroth order in the perturbative expansion) as a functional version of the Magnus expansion.

However, without knowledge of the eigenmodes, the question of the optimal choice for the mode of a local oscillator to be used in homodyne measurements is left open. Since the different eigenmodes are associated with different amounts of squeezing, the optimal amount of squeezing should be obtained when the local oscillator has the same mode as that of the associated eigenmode.

In this paper, we consider the effect of the spatiotemporal properties of the local oscillator directly in terms of the kernels. We perform the calculations with the aid of

*froux@nmisa.org

the Wigner functional formalism [24,25] to all orders in the Magnus expansion of the down-converted state, under the so-called *thin-crystal* approximation. The latter is well satisfied in most experimental conditions, especially when the spatial degrees of freedom play an important role [13]. The effect of higher orders of the Magnus expansion has previously been investigated in four-wave mixing, for the temporal degrees of freedom only [26,27].

Numerous spatiotemporal properties can play a role in homodyne measurements. Here, we consider the effects of the mode size for a Gaussian profile and the temporal bandwidth of the local oscillator. We also consider the effect of the azimuthal index if the local oscillator has a Laguerre-Gauss petal mode profile with zero radial index. The Laguerre-Gauss modal basis is an example of an orbital angular momentum (OAM) basis. Recently, the incorporation of OAM modes into squeezed states has attracted much attention [17,28–31]. Our interest is to determine the effect of the azimuthal index (OAM) on homodyning measurements.

Contrary to our previous work [23], we perform the calculations for the current investigation under the semiclassical approximation only. The validity for this approximation in the current situation, however, is not based on an assumed low efficiency for the down-conversion process. It is justified simply on the assumption that the pump remains a coherent state during the process. As such, the relative size of the minimum uncertainty area of the pump on the functional phase space ensures that it can be adequately approximated with the classical field that parametrizes the coherent state of the pump.

Here, we apply a weak monochromatic assumption: We assume that the pump and the local oscillator both have narrow spectra but finite bandwidths. It allows us to determine the bandwidth of the different terms in the Magnus expansion of the down-converted state, which plays an important role in the results that we obtain.

II. GENERAL APPROACH

In order to determine how successful a strongly driven down-conversion process is at producing a squeezed vacuum state, one can measure the amount of squeezing of the state, using a homodyne measurement. Here, we calculate what would be obtained from such a measurement of the squeezing parameter. It is done by computing the uncertainty (variance) in the measurement of the quadratures of the down-converted state. The variance in the quadrature is given by

$$\sigma_q^2 \equiv \langle \Delta \hat{q}_\theta^2 \rangle = \langle \hat{q}_\theta^2 \rangle - \langle \hat{q}_\theta \rangle^2 = \mathrm{tr}\{\hat{\rho}\hat{q}_\theta^2\} - \mathrm{tr}\{\hat{\rho}\hat{q}_\theta\}^2, \tag{1}$$

where the generalized quadrature operator is defined as

$$\hat{q}_\theta \equiv \hat{q}\cos\theta - \hat{p}\sin\theta, \tag{2}$$

with θ representing the orientation in phase space.

In terms of the spatiotemporal degrees of freedom, a homodyne measurement selects only a specific spatiotemporal mode given by the modulus of the mode of the local oscillator. The phase of the local oscillator determines the orientation of the generalized quadrature operator in phase space. The observable for the homodyne measurement is therefore represented by

$$\hat{h}_\gamma = \sqrt{2}\int |\gamma(\mathbf{k})|\hat{q}_\theta(\mathbf{k})\, đk, \tag{3}$$

where $\gamma(\mathbf{k}) = |\gamma(\mathbf{k})|\exp(i\theta)$[1] represents the parameter function for the coherent state of the local oscillator, $\mathbf{k}$ is the three-dimensional wave vector, and

$$đk \equiv \frac{d^3k}{(2\pi)^3\omega}. \tag{4}$$

We will use a Wigner functional formalism [23,32] to perform the computations. A tutorial for the Wigner functional formalism is provided in the Appendix. The Wigner functional for the homodyne measurement operator is

$$W_{\hat{h}}[\alpha;\gamma] = \gamma^* \diamond \alpha + \alpha^* \diamond \gamma, \tag{5}$$

where the $\diamond$ contraction is defined as

$$\alpha_1^* \diamond \alpha_2 \equiv \int \alpha_1^*(\mathbf{k})\alpha_2(\mathbf{k})\, đk \tag{6}$$

and

$$\alpha(\mathbf{k}) = \frac{1}{\sqrt{2}}[q(\mathbf{k}) + ip(\mathbf{k})] \tag{7}$$

is the complex-valued field variable that parametrizes the functional phase space, with $q(\mathbf{k})$ and $p(\mathbf{k})$ being the eigenvalue functions of the quadrature operators [24,25].

To alleviate the calculation of the expectation values, we define a generating function given by

$$\mathcal{W}(\eta) = \int \exp\left(\eta W_{\hat{h}}[\alpha;\gamma]\right) W_{\hat{\rho}}[\alpha]\, \mathcal{D}^\circ[\alpha], \tag{8}$$

where η is a generating parameter and $W_{\hat{\rho}}[\alpha]$ is the Wigner functional of the state. The expectation values are obtained by computing

$$\begin{aligned} \langle \hat{h}_\gamma \rangle &= \sqrt{2}\gamma_0 \langle \hat{q}_\theta \rangle = \partial_\eta \mathcal{W}(\eta)|_{\eta=0}, \\ \langle \hat{h}_\gamma^2 \rangle &= 2\gamma_0^2 \langle \hat{q}_\theta^2 \rangle = \partial_\eta^2 \mathcal{W}(\eta)|_{\eta=0}, \end{aligned} \tag{9}$$

where

$$\gamma_0^2 = \|\gamma(\mathbf{k})\|^2 \equiv \int |\gamma(\mathbf{k})|^2\, đk. \tag{10}$$

III. SQUEEZED VACUUM STATE

The Wigner functional for the squeezed vacuum state produced by parametric down-conversion is given by [23]

$$W_{\hat{\rho}}[\alpha] = \mathcal{N}_0 \exp(-2\alpha^* \diamond A \diamond \alpha - \alpha \diamond B \diamond \alpha - \alpha^* \diamond B^* \diamond \alpha^*), \tag{11}$$

where $\mathcal{N}_0$ is the normalization constant for the Wigner functional of a pure Gaussian state, and A and B are semiclassical kernel functions associated with the parametric down-conversion process.

[1]Here, it is assumed that the phase is a global constant. In general, it can also be a function of the wave vector $\theta(\mathbf{k})$.

When we substitute Eq. (11) into Eq. (8) and evaluate the functional integral over α, we obtain

$$\begin{aligned}\mathcal{W}(\eta) &= \mathcal{N}_0 \int \exp\left[-2\alpha^* \diamond A \diamond \alpha - \alpha \diamond B^* \diamond \alpha \right.\\ &\quad \left. - \alpha^* \diamond B \diamond \alpha^* + \eta(\gamma^* \diamond \alpha + \alpha^* \diamond \gamma)\right] \mathcal{D}^\circ[\alpha] \\ &= \exp\left(\frac{\eta^2}{2}\gamma^* \diamond A \diamond \gamma - i\frac{\eta^2}{4}\gamma \diamond A^* \diamond B^* \diamond A^{-1} \diamond \gamma \right.\\ &\quad \left. + i\frac{\eta^2}{4}\gamma^* \diamond A^{-1} \diamond B \diamond A^* \diamond \gamma^*\right). \end{aligned} \tag{12}$$

Computing the expectation values, as in Eq. (9), we obtain $\langle \hat{h}_\gamma \rangle = 0$ because the squeezed vacuum state is centered at the origin. The expression for $\langle \hat{h}_\gamma^2 \rangle$ is

$$\begin{aligned}\langle \hat{h}_\gamma^2 \rangle &= \partial_\eta^2 \mathcal{W}(\eta)|_{\eta=0} \\ &= \gamma^* \diamond A \diamond \gamma - i\frac{1}{2}\gamma \diamond A^* \diamond B^* \diamond A^{-1} \diamond \gamma \\ &\quad + i\frac{1}{2}\gamma^* \diamond A^{-1} \diamond B \diamond A^* \diamond \gamma^* \\ &= \gamma^* \diamond A \diamond \gamma - i\frac{1}{2}\gamma \diamond B^* \diamond \gamma + i\frac{1}{2}\gamma^* \diamond B \diamond \gamma^*, \end{aligned} \tag{13}$$

where the final result follows under the assumption that A and B commute and that A is real valued.

IV. SEMICLASSICAL KERNEL FUNCTIONS

Under the semiclassical approximation, the Wigner functional of the down-converted state can be represented in terms of a functional Magnus expansion [18,23], in which the bilinear kernels in the exponent are given by

$$\begin{aligned} A &= \mathbf{1} + \int_0^L \int_0^{z_1} \mathcal{Z}\{H^*(z_1) \diamond H(z_2)\}\, dz_2\, dz_1 \\ &\quad + \int_0^L \int_0^{z_1} \int_0^{z_2} \int_0^{z_3} \mathcal{Z}\{H^*(z_1) \diamond H(z_2) \diamond H^*(z_3) \diamond H(z_4)\}\, dz_4\, dz_3\, dz_2\, dz_1 + \cdots, \\ B &= \int_0^L H(z_1)\, dz_1 + \int_0^L \int_0^{z_1} \int_0^{z_2} \mathcal{Z}\{H(z_1) \diamond H^*(z_2) \diamond H(z_3)\}\, dz_3\, dz_2\, dz_1 \\ &\quad + \int_0^L \int_0^{z_1} \int_0^{z_2} \int_0^{z_3} \int_0^{z_4} \mathcal{Z}\{H(z_1) \diamond H^*(z_2) \diamond H(z_3) \diamond H^*(z_4) \diamond H(z_5)\}\, dz_5\, dz_4\, dz_3\, dz_2\, dz_1 + \cdots. \end{aligned} \tag{14}$$

Here, L is the length of the nonlinear crystal, $H(z)$ is the bilinear vertex kernel that is obtained by contracting the classical parameter function of the pump on the vertex for the down-conversion process, and $\mathcal{Z}\{\cdot\}$ represents a symmetrization operation, which is recursively defined by

$$\mathcal{Z}\{f_1(z_1) \diamond \cdots \diamond f_n(z_n)\} = \tfrac{1}{2} f_1(z_1) \diamond \mathcal{Z}\{f_2(z_2) \diamond \cdots \diamond f_n(z_n)\} + \tfrac{1}{2}\mathcal{Z}\{f_1(z_2) \diamond \cdots \diamond f_{n-1}(z_n)\} \diamond f_n(z_1), \tag{15}$$

with $\mathcal{Z}\{f_1(z_1)\} = f_1(z_1)$. The identity $\mathbf{1}$ is defined so that $\mathbf{1} \diamond \alpha = \alpha$.

The monochromatic parameter function of the pump is assumed to be

$$\zeta(\mathbf{k}) = \zeta_0 w_\mathrm{p} \sqrt{\frac{2\pi\omega}{c}} S(\omega - \omega_\mathrm{p}; \delta\omega_\mathrm{p}) \exp\left(-\frac{1}{4} w_\mathrm{p}^2 |\mathbf{K}|^2\right), \tag{16}$$

where w_p is the beam waist radius, c is the speed of light, $\mathbf{K}$ is the two-dimensional transverse part of $\mathbf{k}$, $S(\omega; \delta\omega)$ is a normalized real-valued spectral function with a bandwidth of $\delta\omega$, and ω_p is the center frequency of the spectrum. The magnitude of the pump's angular spectrum is $\|\zeta(\mathbf{k})\|^2 = |\zeta_0|^2$. The spectral function is normalized:

$$\int S^2(\omega - \omega_\mathrm{p}; \delta\omega_\mathrm{p}) \frac{d\omega}{2\pi} = 1. \tag{17}$$

Under the monochromatic approximation, $S(\omega - \omega_\mathrm{p}; \delta\omega_\mathrm{p})$ is a narrow function centered at ω_p. For the calculations, we model the spectral function as a Gaussian.

For the function in Eq. (16), the bilinear vertex kernel under collinear type I phase matching is

$$\begin{aligned} H(\mathbf{k}_1, \mathbf{k}_2) &= iK_0(\omega_1, \omega_2) S(\omega_\mathrm{p} - \omega_1 - \omega_2; \delta\omega_\mathrm{p}) \\ &\quad \times \exp\left(-\frac{w_\mathrm{p}^2}{4n_\mathrm{p}^2}|n_1\mathbf{K}_1 + n_2\mathbf{K}_2|^2 \right. \\ &\quad \left. + \frac{i3Lcn_1n_2|\omega_2\mathbf{K}_1 - \omega_1\mathbf{K}_2|^2}{2n_\mathrm{p}\omega_\mathrm{p}\omega_1\omega_2}\right), \end{aligned} \tag{18}$$

where $n_\mathrm{p} \equiv n_\mathrm{eff}(\omega_\mathrm{p})$, $n_1 \equiv n_\mathrm{o}(\omega_1)$, $n_2 \equiv n_\mathrm{o}(\omega_2)$, and

$$K_0(\omega_1, \omega_2) = \frac{4\zeta_0^* \sigma_\mathrm{ooe} w_\mathrm{p} \omega_1 \omega_2 \sqrt{2\pi\omega_\mathrm{p}}}{c^3 n_\mathrm{p}^2}, \tag{19}$$

with σ_ooe being the coefficient for the down-conversion process, represented as a scattering cross-section area.

V. THIN CRYSTAL APPROXIMATION

The calculation can be alleviated by employing the *thin crystal approximation*, where the Rayleigh range of the pump

beam is much longer than the length of the nonlinear crystal

$$L \ll \frac{w_\mathrm{p}^2 \omega_\mathrm{p}}{2c}. \tag{20}$$

Such conditions are valid in most parametric down-conversion experiments, especially when the contribution of the spatial degrees of freedom is maximized [13].

The thin crystal approximation is to be separated from the down-conversion efficiency. Therefore, the L's that appear in the exponents of the kernels contribute to the thin crystal approximation, while those outside the exponential functions combine into the down-conversion efficiency and do not play a role in the thin crystal approximation. If we remove the L-dependent part in the exponent of Eq. (18), which means that we only consider the leading-order term in the thin crystal approximation, then the computation of the higher order terms in the Magnus expansions of the semiclassical kernels simplifies. Without the higher order thin crystal contributions in the exponents, the integrals can in some cases become singular. However, in the current analysis, where we overlap the kernels with the parameter function of the local oscillator, such situations do not occur.

The z integrals in the Magnus expansion terms produce factors of $L^n/n!$ for contractions of n bilinear kernels. Hence, the semiclassical kernels can be expressed as

$$\begin{aligned} A &= \mathbf{1} + \sum_{m=1}^{\infty} \frac{L^{2m}}{(2m)!} H_0^{\diamond 2m} \equiv \cosh_\diamond(LH_0), \\ B &= i \sum_{m=1}^{\infty} \frac{L^{2m-1}}{(2m-1)!} H_0^{\diamond(2m-1)} \equiv i \sinh_\diamond(LH_0), \end{aligned} \tag{21}$$

where we set $H_{L=0} \equiv iH_0$.

The integrals associated with the $\diamond$ contractions can be evaluated. For even and odd orders, respectively with $2m$ and $2m-1$ contractions, we obtain

$$\begin{aligned} H_0^{\diamond m_\mathrm{e}} &= \frac{M_\mathrm{e} M_1^{m_\mathrm{e}}}{m_\mathrm{e}^{5/4}} \exp\left(-\frac{1}{4}\frac{w_\mathrm{p}^2 n_1 |\mathbf{K}_1 - \mathbf{K}_2|^2}{m_\mathrm{e} n_\mathrm{p}}\right) \\ &\quad \times S(\omega_1 - \omega_2; \sqrt{m_\mathrm{e}}\delta\omega_\mathrm{p}), \\ H_0^{\diamond m_\mathrm{o}} &= \frac{M_\mathrm{o} M_1^{m_\mathrm{o}}}{m_\mathrm{o}^{5/4}} \exp\left(-\frac{1}{4}\frac{w_\mathrm{p}^2 |n_1 \mathbf{K}_1 + n_2 \mathbf{K}_2|^2}{m_\mathrm{o} n_\mathrm{p}^2}\right) \\ &\quad \times S(\omega_\mathrm{p} - \omega_1 - \omega_2; \sqrt{m_\mathrm{o}}\delta\omega_\mathrm{p}), \end{aligned} \tag{22}$$

where $m_\mathrm{e} \equiv 2m$, $m_\mathrm{o} \equiv 2m-1$, and

$$\begin{aligned} M_\mathrm{e} &= \frac{\pi^{5/4} w_\mathrm{p}^2 n_1^2 \omega_1}{c n_\mathrm{p}^2 \sqrt{\delta\omega_\mathrm{p}}}, \quad M_\mathrm{o} = \frac{\pi^{5/4} w_\mathrm{p}^2 n_1 n_2 \sqrt{\omega_1 \omega_2}}{c n_\mathrm{p}^2 \sqrt{\delta\omega_\mathrm{p}}}, \\ M_1 &= \frac{4|\zeta_0|\sigma_\mathrm{ooe}\sqrt{2\omega_\mathrm{p}\omega_1\omega_2\delta\omega_\mathrm{p}}}{\pi^{3/4} w_\mathrm{p} c^2 n_1 n_2}. \end{aligned} \tag{23}$$

Substituted into Eq. (14), these results lead to explicit expressions for the semiclassical kernels to all orders in the Magnus expansion.

The factors of $1/2m$ and $1/(2m-1)$ in the exponents in Eq. (22) have a significant effect. They cause these functions to become broader for larger m. A similar broadening effect is produced by the factors of $\sqrt{2m}$ and $\sqrt{2m-1}$ that appear with the bandwidths in the spectral functions. These factors appear as a result of the repeated convolutions involved in the multiple contractions and they only become apparent when considering the spatiotemporal degrees of freedom for all the terms in the Magnus expansion. The broadening plays an important role in the parametric process, as we will see below.

VI. QUADRATURE VARIANCE

Since the semiclassical approximation provides us with a Gaussian Wigner functional, the calculation of the variance in quadrature can be performed directly. These kernels commute and A is real valued. Therefore, we can substitute Eq. (21) into Eq. (13) to obtain

$$\begin{aligned} \langle \hat{h}_\gamma^2 \rangle &= \gamma^* \diamond \cosh_\diamond(LH_0) \diamond \gamma - \tfrac{1}{2}\gamma \diamond \sinh_\diamond(LH_0) \diamond \gamma \\ &\quad - \tfrac{1}{2}\gamma^* \diamond \sinh_\diamond(LH_0) \diamond \gamma^*. \end{aligned} \tag{24}$$

First, we consider the case where the parameter function for the local oscillator is a Gaussian angular spectrum with a narrow temporal spectrum. It is given by

$$\begin{aligned} \gamma(\mathbf{k}) &= \gamma_0 w_0 \sqrt{\frac{2\pi\omega}{c}} \Phi_0 S_0(\omega - \omega_\mathrm{d}; \delta\omega_\mathrm{d}) \\ &\quad \times \exp\left(-\frac{1}{4} w_0^2 |\mathbf{K}|^2\right), \end{aligned} \tag{25}$$

where w_0 is the local oscillator beam waist radius, imaged to the crystal plane, $\Phi_0 = \exp(i\theta)$, and $S_0(\omega - \omega_\mathrm{d}; \delta\omega_\mathrm{d})$ is a narrow spectral function with a bandwidth $\delta\omega_\mathrm{d}$, modeled as a Gaussian function centered at the degenerate down-conversion frequency ω_d.

We substitute Eq. (22) into Eq. (21) and then, together with Eq. (25), into Eq. (13). After evaluating the integrals, we obtain the quadrature variance

$$\begin{aligned} \sigma_q^2 = \frac{\langle \hat{h}_\gamma^2 \rangle}{2\gamma_0^2} &= \frac{1}{2} + \sum_{m=1}^{\infty} \frac{\Xi^{2m}(1+m\xi)^{-1/2}}{2(1+m\tau)(2m)!} \\ &\quad + \sin(2\theta) \sum_{m=1}^{\infty} \frac{\Xi^{2m-1}\left[1 + \frac{1}{2}(2m-1)\xi\right]^{-1/2}}{[2+(2m-1)\tau](2m-1)!}, \end{aligned} \tag{26}$$

where

$$\xi \equiv \frac{\delta\omega_\mathrm{p}^2}{\delta\omega_\mathrm{d}^2}, \quad \tau \equiv \frac{n_\mathrm{p}^2 w_0^2}{n_\mathrm{d}^2 w_\mathrm{p}^2}, \tag{27}$$

with $n_\mathrm{d} \equiv n_\mathrm{o}(\omega_\mathrm{d})$ and

$$\Xi \equiv \frac{2^{7/2}\pi^{5/4} L |\zeta_0| \sigma_\mathrm{ooe} \sqrt{\delta_\mathrm{p}}}{w_\mathrm{p} n_\mathrm{d}^2 \lambda_\mathrm{p}^2}, \tag{28}$$

represent the efficiency of the down-conversion process, with the fractional bandwidth defined by

$$\delta_\mathrm{p} \equiv \frac{\delta\lambda_\mathrm{p}}{\lambda_\mathrm{p}} = \frac{\delta\omega_\mathrm{p}}{\omega_\mathrm{p}}. \tag{29}$$

The dimensionless quantity ξ represents the squared ratio of the bandwidths of the pump and the down-converted light.

These bandwidths are respectively determined by the properties of the pump source and the spectral filters used before the detection of the down-converted light. The dimensionless

quantity τ is the squared ratio of the beam widths of the local oscillator and the pump in the crystal plane, combined with their associated refractive indices. Both ξ and τ are controllable in terms of the chosen experimental parameters.

A. Small ξ and small τ

The standard result of squeezing behavior is obtained when we assume that $w_p \gg w_0$ and $\delta\omega_d \gg \delta\omega_p$, so that $\xi \to 0$ and $\tau \to 0$. These conditions reproduce the well-known result

$$\sigma_q^2 = \frac{1}{2} + \frac{1}{2}\sum_{m=1}^{\infty}\frac{\Xi^{2m}}{(2m)!} + \frac{1}{2}\sin(2\theta)\sum_{m=1}^{\infty}\frac{\Xi^{2m-1}}{(2m-1)!}$$
$$= \frac{1}{2}\cosh(\Xi) + \frac{1}{2}\sin(2\theta)\sinh(\Xi). \tag{30}$$

The phase of the local oscillator is used to select two special orientations in phase space. For $\sin(2\theta) = \pm 1$,

$$\sigma_\pm^2 = \tfrac{1}{2}\exp(\pm\Xi). \tag{31}$$

These orientations represent those along which the Wigner functional has is maximum and minimum variance, respectively—i.e., the squeezing direction and the direction orthogonal to it. The down-conversion efficiency Ξ, given in Eq. (28), is identified as the squeezing parameter. The product of the standard deviations along these orientations is a constant

$$\sigma_+\sigma_- = \tfrac{1}{2}, \tag{32}$$

which indicates that the part of the state that is observed in the homodyne experiment remains a minimum uncertainty state, regardless of the amount of squeezing.

In a practical situation, ξ and τ will have finite values. Even if they are small, there will be a point where m becomes large enough so that the approximations $\xi \to 0$ and $\tau \to 0$ are not valid anymore. Next, we will consider the effect of these two cases in turn.

B. Small ξ and arbitrary τ

Here we still assume $\xi \to 0$, but consider arbitrary τ. For $\xi = 0$, $\tau > 0$, and $\sin(2\theta) = \pm 1$, the variance becomes

$$\sigma_\pm^2 = \sum_{n=0}^{\infty}\frac{(\pm\Xi)^n}{(n\tau+2)n!} = \frac{1}{2}{}_1F_1\left(\frac{2}{\tau};1+\frac{2}{\tau};\pm\Xi\right), \tag{33}$$

where ${}_1F_1$ is a hypergeometric function. The result is that the squeezing effect is reduced. In Fig. 1, the curves for minimum variance σ_-^2 are shown as a function of the squeezing parameter Ξ for different values of τ. It demonstrates the increase in the minimum variance as the value of τ increases.

The observed size of the uncertainty area is shown in Fig. 2, as a function of the squeezing parameter Ξ for the same values of τ shown in Fig. 1. We see that, for $\tau > 0$, the observed part of the state loses its minimum uncertainty property:

$$\sigma_+\sigma_- > \tfrac{1}{2}. \tag{34}$$

It is interesting to note that the increase in the size of the uncertainty area is not a monotonous function of τ. In Fig. 3, the uncertainty area is shown as a function of τ for different values of the squeezing parameter Ξ. It shows that the size of the uncertainty area peaks around $\tau \approx 6$ and then decreases again.

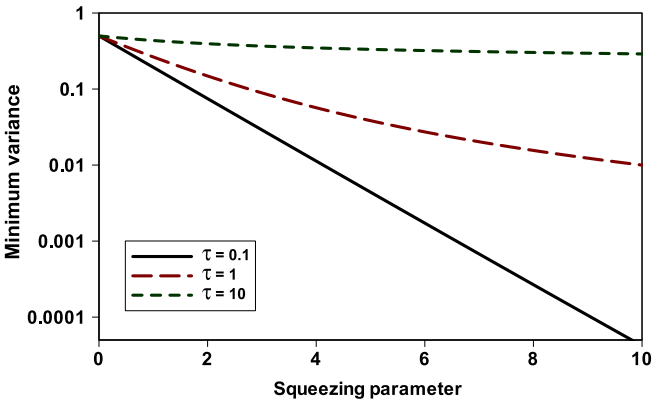

FIG. 1. The minimum variance σ_-^2 is plotted as a function of the squeezing parameter Ξ for $\tau = 0.1$, $\tau = 1$, and $\tau = 10$.

C. Small τ and arbitrary ξ

For the opposite situation, we assume $\tau \to 0$ and consider arbitrary ξ. For $\tau = 0$, $\xi > 0$, and $\sin(2\theta) = \pm 1$, we obtain a result that cannot be summed:

$$\sigma_\pm^2 = \sum_{n=0}^{\infty}\frac{(\pm\Xi)^n}{n!\sqrt{2}\sqrt{2+n\xi}}. \tag{35}$$

However, with the aid of the auxiliary integral,

$$\frac{1}{\sqrt{a}} = \frac{1}{\sqrt{\pi}}\int \exp(-ax^2)\,dx, \tag{36}$$

we can represent it as an integral, given by

$$\sigma_\pm^2 = \int \frac{\exp(-2x^2)}{\sqrt{2\pi}}\exp[\pm\Xi\exp(-\xi x^2)]\,dx. \tag{37}$$

It can be seen as an ensemble average of different curves with squeezing parameters varying as $\Xi\exp(-\xi x^2)$ for a Gaussian probability density. The effect of the ensemble averaging is to diminish the squeezing effect, depending on the value of ξ. If $\xi \ll 2$, the ensemble averaging effect is negligible, and one can set $\xi = 0$.

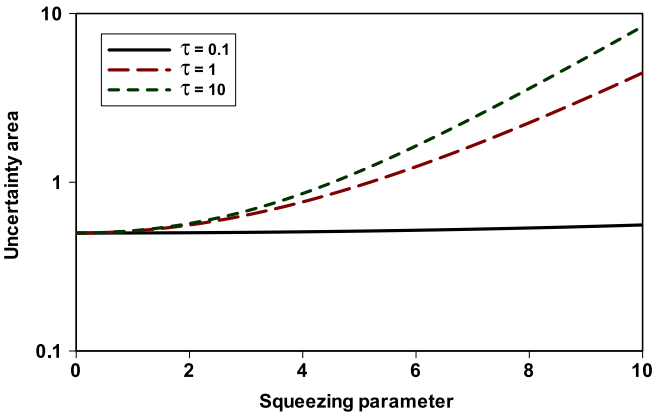

FIG. 2. The uncertainty area size $\sigma_+\sigma_-$ as a function of the squeezing parameter Ξ for $\tau = 0.1$, $\tau = 1$, and $\tau = 10$.

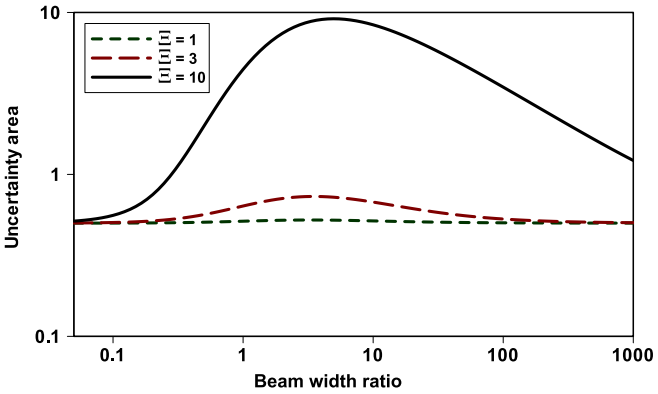

FIG. 3. The uncertainty area size $\sigma_+\sigma_-$ as a function of the beam width ratio τ for $\Xi = 1$, $\Xi = 3$, and $\Xi = 10$.

In the case where both ξ and τ can have arbitrary values, one would have a combination of these two effects. Hence, the optimal experimental conditions are those where $w_\mathrm{p} \gg w_0$ and $\delta\omega_\mathrm{d} \gg \delta\omega_\mathrm{p}$.

VII. LAGUERRE-GAUSS LOCAL OSCILLATOR

Next, we consider the effect of using the Laguerre-Gauss modal basis for the local oscillator profile. Since the down-converted photon pairs under collinear phase-matching conditions maintain the angular momentum of the pump photons that produced them, the azimuthal index of the one photon would always be the opposite of the other photon, if the pump has a zero azimuthal index. As a result, a local oscillator profile consisting of only one Laguerre-Gauss mode would only be able to see one of the two photons in a down-converted pair. Both photons are necessary for the squeezing effect. Therefore, such a single Laguerre-Gauss mode local oscillator would not see any squeezing.

For this reason, we consider petal modes that are formed as the superposition of two Laguerre-Gauss modes with opposite azimuthal indices. In terms of their angular spectra, the superposition is given by

$$\phi^{(\mathrm{petal})}_{|\ell|,p}(\mathbf{k}) = \frac{1}{\sqrt{2}}\phi^{(\mathrm{LG})}_{\ell,p}(\mathbf{k}) + \frac{1}{\sqrt{2}}\phi^{(\mathrm{LG})}_{-\ell,p}(\mathbf{k}). \tag{38}$$

Note that a relative phase between the two Laguerre-Gauss modes would only produce an ineffectual rotation of the petal mode. Therefore, we do consider such a relative phase.

To alleviate the calculation, we use a generating function for the angular spectra of the Laguerre-Gauss modes, given by [33,34]

$$\mathcal{G}(\mathbf{k},\mu,\nu,s) = \frac{w_0\mathcal{N}_{\ell,p}}{1+\nu}\exp\left[\frac{iw_0(k_x+isk_y)\mu}{2(1+\nu)}\right] \times \exp\left[-\frac{w_0^2(k_x^2+k_y^2)(1-\nu)}{4(1+\nu)}\right], \tag{39}$$

where μ and ν are generating parameters for the azimuthal and radial indices ℓ and p, respectively, and s is a sign that represents the sign of the azimuthal index. The normalization constant is given by

$$\mathcal{N}_{\ell,p} = \sqrt{\frac{2^{|\ell|-1}p!}{\pi(p+|\ell|)!}}. \tag{40}$$

The mode of the local oscillator is now defined in terms of the generating function:

$$\gamma(\mathbf{k},\mu,\nu,s) = 2\pi\Phi_0\gamma_0 w_0\sqrt{\frac{\omega}{c}}S_0(\omega-\omega_\mathrm{d};\delta\omega_\mathrm{d})\mathcal{G}(\mathbf{k},\mu,\nu,s). \tag{41}$$

The construction of the petal modes from this generating function is left until after the calculations.

The expression in Eq. (41) is substituted into Eq. (24), together with the expansions of the kernels in Eq. (22). Since the generating function in Eq. (41) appears twice in each term, two different sets of generating parameters need to be used: $\{\mu_1,\nu_1,s_1\}$ and $\{\mu_2,\nu_2,s_2\}$. After evaluating all the integrals, we obtain

$$\mathcal{J} = 2\pi\mathcal{N}_{\ell,p}\sum_{m=0}^{\infty}\left\{\frac{\Xi^{2m}(1+m\xi)^{-1/2}}{d_\mathrm{e}(\nu_1,\nu_1,\tau)(2m)!}\exp\left[\frac{\mu_1\mu_2(1+s_1s_2)}{2d_\mathrm{e}(\nu_1,\nu_1,\tau)}\right] \pm \frac{\Xi^{2m+1}\left[1+\frac{1}{2}(2m+1)\xi\right]^{-1/2}}{d_\mathrm{o}(\nu_1,\nu_1,\tau)(2m+1)!}\exp\left[\frac{\mu_1\mu_2(1-s_1s_2)}{2d_\mathrm{o}(\nu_1,\nu_1,\tau)}\right]\right\}, \tag{42}$$

where

$$\begin{aligned} d_\mathrm{e}(\nu_1,\nu_1,\tau) &\equiv 2m(1-\nu_1)(1-\nu_2)\tau + 2(1-\nu_1\nu_2), \\ d_\mathrm{o}(\nu_1,\nu_1,\tau) &\equiv (2m+1)(1-\nu_1)(1-\nu_2)\tau \\ &\quad + 2(1-\nu_1\nu_2). \end{aligned} \tag{43}$$

If the local oscillator consists of one Laguerre-Gauss mode only, we must set $s_1 = s_2$, which implies that the second term in Eq. (42) becomes independent of μ_1 and μ_2. Therefore, only the first term survives for $|\ell| > 0$, leading to no squeezing.

At this point, we produce the petal modes by producing superpositions for both $s_1 = \pm 1$ and $s_2 = \pm 1$. The result then becomes

$$\mathcal{J}' = \sum_{m=0}^{\infty}\frac{2\pi\mathcal{N}_{\ell,p}(\pm\Xi)^m\left(1+\frac{1}{2}m\xi\right)^{-1/2}}{[m(1-\nu_1)(1-\nu_2)\tau + 2(1-\nu_1\nu_2)]m!} \times \exp\left[\frac{\mu_1\mu_2}{m(1-\nu_1)(1-\nu_2)\tau + 2(1-\nu_1\nu_2)}\right]. \tag{44}$$

If we assume $\xi \to 0$ and $\tau \to 0$, the expression reverts back to that for ideal squeezing, independent of ℓ and p. Therefore, under such conditions, the petal basis still supports squeezing in the same way one finds for $\ell = 0$.

We will assume $\xi \to 0$ but allow arbitrary values for τ. We also set the radial index to zero $p = 0$, which is equivalent to setting $\nu_1 = \nu_2 = 0$. The resulting expression for the generating function can then be used to generate the variance for arbitrary $|\ell|$:

$$\sigma_\pm^2 = \sum_{n=0}^{\infty}\frac{(\pm\Xi)^n 2^{|\ell|}}{(n\tau+2)^{|\ell|+1}n!}. \tag{45}$$

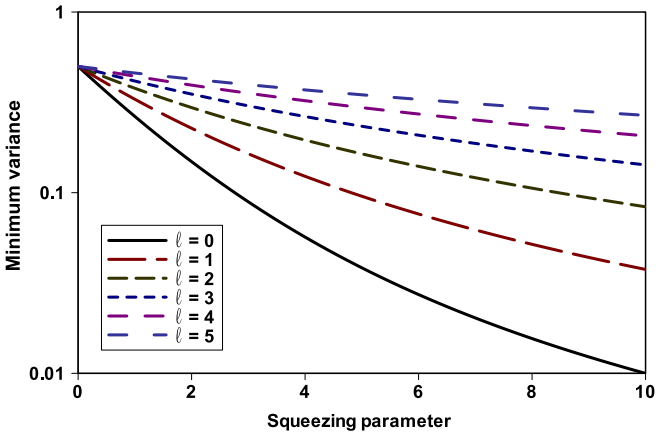

FIG. 4. The minimum variance σ_-^2 is plotted as a function of the squeezing parameter Ξ for $\tau = 1$ and $\ell = 0 \ldots 5$.

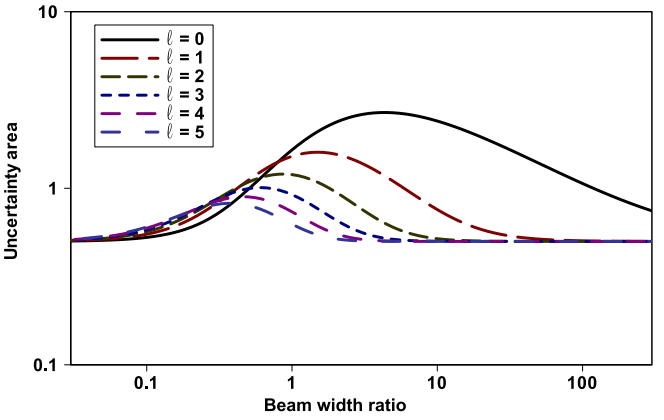

FIG. 6. The uncertainty area size $\sigma_+\sigma_-$ as a function of the beam width ratio τ at $\Xi = 7$ for $\ell = 0 \ldots 5$.

It reproduces Eq. (33) for $\ell = 0$, as expected. After evaluating the summation, we obtain the hypergeometric function

$$\sigma_\pm^2 = \tfrac{1}{2}{}_tF_t(M, \ldots, M; N, \ldots, N; \pm\Xi), \tag{46}$$

where $t = |\ell| + 1$, $M = 2/\tau$, and $N = 1 + 2/\tau$. The sequences of M's and N's in the argument of the hypergeometric function denote $|\ell| + 1$ entries each.

The minimum variance obtained when using a local oscillator with such petal mode profiles are shown in Fig. 4 as a function of the squeezing parameter Ξ for different values of the azimuthal index ℓ and with $\tau = 1$. The rate of decrease in the minimum width slows down for larger azimuthal index.

The curves of the uncertainty area for these petal mode profiles are shown in Fig. 5 as a function of the squeezing parameter Ξ for different values of the azimuthal index ℓ and with $\tau = 1$. It is surprising to see that the uncertainty area increases more slowly for higher azimuthal indices than for lower azimuthal indices.

We also consider the size of the uncertainty area as a function of the parameter τ. In Fig. 6, it is shown for different values of the azimuthal index ℓ at $\Xi = 7$. Again, we note that the size of the uncertainty area reaches a peak for a certain value of τ that depends on the azimuthal index ℓ and decreases for larger values of τ.

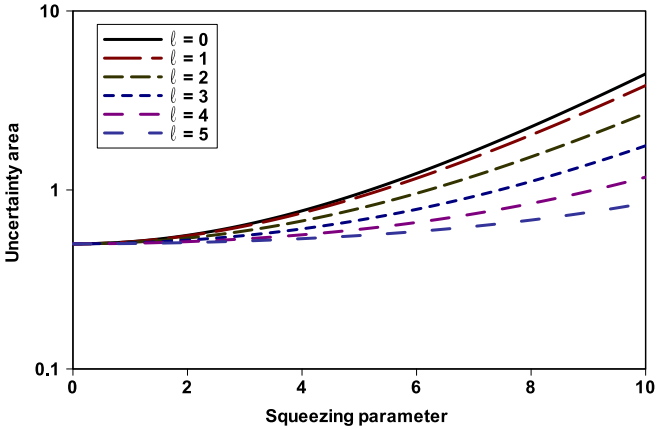

FIG. 5. The uncertainty area size $\sigma_+\sigma_-$ as a function of the squeezing parameter Ξ for $\tau = 1$ and $\ell = 0 \ldots 5$.

VIII. DISCUSSION

The effect of selected spatiotemporal properties of the local oscillator on the measurement of squeezing on a parametric down-converted state is investigated. The calculations are done directly in terms of the kernel functions and not on matrices derived from these kernel functions, which would require knowledge of the eigenbasis of the process. It makes it possible to perform calculations to all orders in the Magnus expansion of the down-converted state under thin crystal conditions.

The calculation demonstrates the efficacy of the Wigner functional approach: It incorporates all the spatiotemporal degrees of freedom without the need for discretization, which would require truncation to obtain explicit results. Yet, it contains all the relevant experimental parameters to make the analytically calculated result suitable for comparison with experimental results.

The Wigner functional approach reveals a progressive broadening of the angular spectra and spectral functions for higher order terms in the Magnus expansion. The observed effect of the broadening depends on the experimental parameters of the local oscillator used for homodyne measurements of the amount of squeezing.

When the spatiotemporal degrees of freedom are ignored in analyses of the down-conversion process, one obtains the ideal squeezing behavior. Such ideal behavior is also seen in those analyses that incorporate the spatiotemporal degrees of freedom, but only goes as far as the first-order term in the Magnus expansion [18]. It is only analyses that consider higher order terms in the Magnus expansion that would reveal the broadening in the widths of the angular spectra and spectral functions, leading to a reduction in the squeezing effect.

We investigate the parameter dependence of the reduction in squeezing, which deviates from the ideal squeezing behavior. It is found that, to get as close to the ideal squeezing behavior as possible, the mode size of the local oscillator should be as small as possible compared to the mode size of

the pump and the bandwidth of the local oscillator should be much larger than that of the pump.

We also consider the effect of the azimuthal index when the local oscillator has a petal mode structure composed of the superposition of the Laguerre-Gauss mode with opposite azimuthal index. It is found that for a finite beam width ratio, the best squeezing behavior is obtained when the azimuthal index is zero.

Some interesting observations emerged from this investigation. The uncertainty area of the part of the squeezed vacuum state that is observed at first increases as the beam width ratio increases, but then it starts to decrease again for further increases in the beam width ratio. We also found that although the minimum variance is better for smaller azimuthal indices, the size of the uncertainty area increases faster for smaller azimuthal indices.

ACKNOWLEDGMENT

This work was supported in part by funding from the National Research Foundation of South Africa (Grant No. 118532).

APPENDIX: WIGNER FUNCTIONAL FORMALISM FOR QUANTUM OPTICS

The Wigner functionals for quantum optics [23–25,32] is formulated in terms of quadrature bases that are obtained as eigenstates of the wave vector dependent quadrature operators,

$$\hat{q}_s(\mathbf{k})|q\rangle = |q\rangle q_s(\mathbf{k}), \quad \hat{p}_s(\mathbf{k})|p\rangle = |p\rangle p_s(\mathbf{k}), \tag{A1}$$

which are defined in terms of the ladder operators,

$$\hat{q}_s(\mathbf{k}) = \frac{1}{\sqrt{2}}[\hat{a}_s(\mathbf{k}) + \hat{a}_s^\dagger(\mathbf{k})],$$
$$\hat{p}_s(\mathbf{k}) = \frac{-i}{\sqrt{2}}[\hat{a}_s(\mathbf{k}) - \hat{a}_s^\dagger(\mathbf{k})]. \tag{A2}$$

The subscript s represents the spin degrees of freedom. To simplify notation, the spin is henceforth neglected; it can be readily reintroduce, if necessary.

While the quadrature operators are unique operator-valued functions of the wave vector, there are an infinite number of the real-valued eigenvalue functions $q(\mathbf{k})$ and $p(\mathbf{k})$, such that $q, p \in L^2\{\mathbb{R}^3\}$. There is a unique eigenstate $|q\rangle$ or $|p\rangle$ associated with each eigenvalue function $q(\mathbf{k})$ or $p(\mathbf{k})$. The quadrature eigenstates form complete orthogonal bases for the entire Hilbert space of all quantum optical states [24,25]. These completeness and orthogonality relationships require integrations over the space of all real-valued eigenvalue functions, thus leading to a functional integral formulation.

To alleviate the notational burden of such functional expressions, we introduce a binary operator denoted by $\diamond$ and call it a $\diamond$ *contraction*. For the inner product between two functions, the $\diamond$ contraction is represented by

$$\langle f, g\rangle \equiv \int f^*(\mathbf{k}) g(\mathbf{k})\, đk \equiv f^* \diamond g. \tag{A3}$$

When there is a kernel function involved, we have

$$f^* \diamond B \diamond g \equiv \int f^*(\mathbf{k}) B(\mathbf{k}, \mathbf{k}') g(\mathbf{k}')\, đk\, đk'. \tag{A4}$$

However, note that

$$f^* \diamond T \diamond g \neq \int f^*(\mathbf{k}) T(\mathbf{k}) g(\mathbf{k})\, đk. \tag{A5}$$

An important quantity is the overlap $\langle q|p\rangle$, which reads

$$\langle q|p\rangle = \exp\left[i \int q(\mathbf{k}) p(\mathbf{k}) đk\right] \equiv \exp(iq \diamond p). \tag{A6}$$

It indicate that the quadrature bases are related by functional Fourier transforms.

It is convenient to combine the real-valued eigenvalue functions of $q(\mathbf{k})$ and $p(\mathbf{k})$ as

$$\alpha(\mathbf{k}) = \frac{1}{\sqrt{2}}[q(\mathbf{k}) + ip(\mathbf{k})]. \tag{A7}$$

The resulting complex-valued function represents the *field variable* for the functional phase space on which quasidistribution functionals are defined.

Using the orthogonality relationships of the quadrature bases, one can show that

$$\int \exp\left(\alpha_0^* \diamond \alpha - \alpha^* \diamond \alpha_0\right) \mathcal{D}^\circ[\alpha] = (2\pi)^\Omega \delta[\alpha_0], \tag{A8}$$

where α_0 is an independent field variable. The measure of the functional integral combines those for the two quadrature bases,

$$\mathcal{D}^\circ[\alpha] \equiv \mathcal{D}\left[q, \frac{p}{2\pi}\right]. \tag{A9}$$

It indicates that the functional integration is performed over the space of all finite-energy angular spectral functions. The Dirac δ functional with the complex-valued argument is defined as the product of those for the two real-valued functions,

$$\delta[\alpha_0] \equiv \delta[q_0]\, \delta[p_0]. \tag{A10}$$

The constant $(2\pi)^\Omega$ is formally divergent, because Ω is a cardinal number representing the number of degrees of freedom of the functional space. These divergent constants are inevitable for properly normalized states defined on functional phase space. However, they would cancel for any physically observable quantity.

The generic functional integral with an integrand in isotropic Gaussian form can be evaluated to give

$$\int \exp\left(-\alpha^* \diamond K \diamond \alpha - \alpha^* \diamond \xi - \zeta^* \diamond \alpha\right) \mathcal{D}^\circ[\alpha]$$
$$= \frac{\exp\left(\zeta^* \diamond K^{-1} \diamond \xi\right)}{\det\{K\}}, \tag{A11}$$

where K is an invertible kernel, and ξ and ζ are complex functions. The functional determinant is given by

$$\det\{K\} = \exp[\mathrm{tr}\{\ln_\diamond(K)\}], \tag{A12}$$

where $\ln_\diamond(\cdot)$ is defined as the inverse of

$$\exp_\diamond(H) \equiv \mathbf{1} + H + \frac{1}{2} H \diamond H + \cdots = \mathbf{1} + \sum_{n=1}^{\infty} \frac{1}{n!} (H)^{\diamond n}, \tag{A13}$$

for an arbitrary kernel function $H(\mathbf{k}_1, \mathbf{k}_2)$, and the trace of such a kernel is given by

$$\mathrm{tr}\{H\} \equiv \int H(\mathbf{k}, \mathbf{k})\, đk. \tag{A14}$$

The Wigner functional is now defined by

$$W_{\hat{A}}[\alpha] \equiv \int \left\langle q + \frac{1}{2}x \middle| \hat{A} \middle| q - \frac{1}{2}x \right\rangle \exp(-ip \diamond x)\, \mathcal{D}[x], \tag{A15}$$

where x is a real-valued integration field variable and $\hat{A}$ is an operator on the Hilbert space of all quantum optical states, incorporating both particle-number degrees of freedom and spatiotemporal degrees of freedom.

The trace of the operator is represented by the functional integral of its associated Wigner functional, which gives 1 if $\hat{A}$ is a density operator $\hat{\rho}$,

$$\mathrm{tr}\{\hat{\rho}\} = \int W_{\hat{\rho}}[\alpha]\, \mathcal{D}^\circ[\alpha] = 1. \tag{A16}$$

As a quasiprobability distribution over the functional phase space, the Wigner functional of a state does not qualify as a true probability density. However, one can compute a probability density (the marginal distributions) from it by integrating over either p or q (or any linear combination of p and q):

$$\int W[q, p]\, \mathcal{D}\left[\frac{p}{2\pi}\right] = \langle q|\hat{\rho}|q\rangle = \rho[q, q],$$
$$\int W[q, p]\, \mathcal{D}[q] = \langle p|\hat{\rho}|p\rangle = \rho[p, p]. \tag{A17}$$

If we integrate these marginal probability distributions over the remaining variables, we obtain 1, thanks to the normalization.

[1] R. Loudon and P. L. Knight, Squeezed light, J. Mod. Opt. **34**, 709 (1987).

[2] A. I. Lvovsky, Squeezed light, Photon. Sci. Found., Technol. Appl. **1**, 121 (2015).

[3] M. I. Kolobov, The spatial behavior of nonclassical light, Rev. Mod. Phys. **71**, 1539 (1999).

[4] S. L. Braunstein, Squeezing as an irreducible resource, Phys. Rev. A **71**, 055801 (2005).

[5] C. Weedbrook, S. Pirandola, R. García-Patrón, N. J. Cerf, T. C. Ralph, J. H. Shapiro, and S. Lloyd, Gaussian quantum information, Rev. Mod. Phys. **84**, 621 (2012).

[6] S. L. Braunstein and P. Van Loock, Quantum information with continuous variables, Rev. Mod. Phys. **77**, 513 (2005).

[7] G. Adesso, S. Ragy, and A. R. Lee, Continuous variable quantum information: Gaussian states and beyond, Open Syst. Inf. Dyn. **21**, 1440001 (2014).

[8] U. L. Andersen, T. Gehring, C. Marquardt, and G. Leuchs, 30 years of squeezed light generation, Phys. Scr. **91**, 053001 (2016).

[9] J. Aasi, J. Abadie, B. P. Abbott, R. Abbott, T. D. Abbott, M. R. Abernathy, C. Adams, T. Adams, P. Addesso, R. X. Adhikari *et al.*, Enhanced sensitivity of the LIGO gravitational wave detector by using squeezed states of light, Nat. Photon. **7**, 613 (2013).

[10] C. K. Hong and L. Mandel, Theory of parametric frequency down conversion of light, Phys. Rev. A **31**, 2409 (1985).

[11] H. H. Arnaut and G. A. Barbosa, Orbital and Intrinsic Angular Momentum of Single Photons and Entangled Pairs of Photons Generated by Parametric Down-Conversion, Phys. Rev. Lett. **85**, 286 (2000).

[12] R. S. Bennink and R. W. Boyd, Improved measurement of multimode squeezed light via an eigenmode approach, Phys. Rev. A **66**, 053815 (2002).

[13] C. K. Law and J. H. Eberly, Analysis and Interpretation of High Transverse Entanglement in Optical Parametric Down Conversion, Phys. Rev. Lett. **92**, 127903 (2004).

[14] F. M. Miatto, H. D. L. Pires, S. M. Barnett, and M. P. van Exter, Spatial Schmidt modes generated in parametric down-conversion, Eur. Phys. J. D **66**, 263 (2012).

[15] A. Gatti, T. Corti, E. Brambilla, and D. B. Horoshko, Dimensionality of the spatiotemporal entanglement of parametric down-conversion photon pairs, Phys. Rev. A **86**, 053803 (2012).

[16] S. P. Walborn, C. H. Monken, S. Pádua, and P. H. Souto Ribeiro, Spatial correlations in parametric down-conversion, Phys. Rep. **495**, 87 (2010).

[17] R. N. Lanning, Z. Xiao, M. Zhang, I. Novikova, E. E. Mikhailov, and J. P. Dowling, Quantized nonlinear Gaussian-beam dynamics: Tailoring multimode squeezed-light generation, Phys. Rev. A **98**, 043824 (2018).

[18] D. B. Horoshko, L. La Volpe, F. Arzani, N. Treps, C. Fabre, and M. I. Kolobov, Bloch-Messiah reduction for twin beams of light, Phys. Rev. A **100**, 013837 (2019).

[19] C. Bloch and A. Messiah, The canonical form of an antisymmetric tensor and its application to the theory of superconductivity, Nucl. Phys. **39**, 95 (1962).

[20] W. Magnus, On the exponential solution of differential equations for a linear operator, Commun. Pure Appl. Math. **7**, 649 (1954).

[21] S. Blanes, F. Casas, J. A. Oteo, and J. Ros, The Magnus expansion and some of its applications, Phys. Rep. **470**, 151 (2009).

[22] D. Barral, N. Belabas, L. M. Procopio, V. d'Auria, S. Tanzilli, K. Bencheikh, and J. A. Levenson, Continuous-variable entanglement of two bright coherent states that never interacted, Phys. Rev. A **96**, 053822 (2017).

[23] F. S. Roux, Parametric down-conversion beyond the semiclassical approximation, Phys. Rev. Research **2**, 033398 (2020).

[24] F. S. Roux, Combining spatiotemporal and particle-number degrees of freedom, Phys. Rev. A **98**, 043841 (2018).

[25] F. S. Roux, Erratum: Combining spatiotemporal and particle-number degrees of freedom [Phys. Rev. A 98, 043841 (2018)], Phys. Rev. A **101**, 019903(E) (2020).

[26] N. Quesada and J. E. Sipe, Effects of time ordering in quantum nonlinear optics, Phys. Rev. A **90**, 063840 (2014).

[27] N. Quesada and J. E. Sipe, Time-Ordering Effects in the Generation of Entangled Photons Using Nonlinear Optical Processes, Phys. Rev. Lett. **114**, 093903 (2015).

[28] M. Lassen, G. Leuchs, and U. L. Andersen, Continuous Variable Entanglement and Squeezing of Orbital Angular Momentum States, Phys. Rev. Lett. **102**, 163602 (2009).

[29] M. T. L. Hsu, W. P. Bowen, and P. K. Lam, Spatial-state Stokes-operator squeezing and entanglement for optical beams, Phys. Rev. A **79**, 043825 (2009).

[30] A. Pecoraro, F. Cardano, L. Marrucci, and A. Porzio, Continuous-variable entangled states of light carrying orbital angular momentum, Phys. Rev. A **100**, 012321 (2019).

[31] J.-D. Zhang, C.-F. Jin, Z.-J. Zhang, L.-Z. Cen, J.-Y. Hu, and Y. Zhao, Super-sensitive angular displacement estimation via an SU(1,1)-SU(2) hybrid interferometer, Opt. Express **26**, 33080 (2018).

[32] F. S. Roux, Quantifying entanglement of parametric down-converted states in all degrees of freedom, Phys. Rev. Research **2**, 023137 (2020).

[33] F. S. Roux, Infinitesimal-propagation equation for decoherence of an orbital-angular-momentum-entangled biphoton state in atmospheric turbulence, Phys. Rev. A **83**, 053822 (2011).

[34] C. M. Mabena and F. S. Roux, Optical orbital angular momentum under strong scintillation, Phys. Rev. A **99**, 013828 (2019).